Measurement 135 (2019) 438–451

Contents lists available at ScienceDirect

Measurement

journal homepage: www.elsevier.com/locate/measurement

New machine learning-based prediction models for fracture energy of asphalt mixtures

Hamed Majidifard, Behnam Jahangiri, William G. Buttlar, Amir H. Alavi *

Department of Civil and Environmental Engineering, University of Missouri, Columbia, USA

ARTICLE INFO

Article history:
Received 21 September 2018
Received in revised form 12 November 2018
Accepted 26 November 2018
Available online 28 November 2018

Keywords:
Fracture energy
Asphalt concrete
Disk-shaped compact tension test
Machine learning
Prediction

ABSTRACT

This paper presents innovative machine learning methods called gene expression programming (GEP) and hybrid artificial neural network/simulated annealing (ANN/SA) to predict the fracture energy of asphalt mixture specimens. The GEP and ANN/SA models are developed using an experimental database including a number of disk-shaped compact tension (DC(T)) test results for fracture energy. The fracture energy is formulated in terms of various predictor variables such as asphalt binder performance grading (PG), asphalt content, aggregate size, aggregate gradation, reclaimed asphalt pavement (RAP) content, reclaimed asphalt shingles (RAS) content, crumb rubber content, and test temperature. A calculation procedure is presented to interpret the models and transform them into practical design equations. A sensitivity analysis is conducted to evaluate the effect of these predictor variables on the fracture energy. Based on the results, the proposed design equations accurately characterize the fracture energy of asphalt mixtures. The GEP model appears to be more practical than the ANN/SA model because of its better generalization and simpler functional structure. The models are recommended for pre-design purposes or as a means to determine asphalt mixture fracture energy when testing is not feasible.

© 2018 Elsevier Ltd. All rights reserved.

1. Introduction

Cracking is one of the principal distresses in asphalt pavements. This phenomenon can be classified into two main categories: load-associated and non-load-associated cracking. Fatigue cracking belongs to the first category. It occurs when tensile stresses due to repetitive traffic loading exceed the tensile strength of the material. As a result of excessive tensile stress, micro-cracks form, grow, and incorporate into macro-cracks leading to aggregate cracking and pavement structural failure [70]. Thermal cracking or low-temperature cracking is a major non-load-associated asphalt pavement distress in cold climates [53]. As the temperature drops, thermal stresses develop due to the differential contraction of the binder and aggregate in the asphalt mastic. In addition, the pavement tends to develop longitudinal tensile strain due to restrained contraction caused by decreasing temperatures [33,55,56]. Continuous construction (infrequent transverse joints) and bonding to underlying layers creates the aforementioned restraint. If the thermal stresses exceed the tensile strength of the asphalt mixture, transversely-oriented, thermal cracks can form (see Fig. 1). Reflective cracking is also a common distress in asphalt pavement surfaces, driven by stress concentrations resulting from the placement of a continuous asphalt overlay on top of a discontinuous pavement (such as jointed concrete pavement, or deteriorated, cracked pavement).

The most widely-used tests to evaluate the thermal cracking resistance of asphalt mixtures are thermal stress restrained specimen test (TSRST), indirect tensile creep and strength test (IDT), semi-circular bending (SCB) test, and disc-shaped compact tension (DC(T)) test. Two main features of the DC(T) test is that it allows for testing cylindrical cores obtained from the field or compacted Superpave Gyratory Compacter (SGC) specimens, and its large fracture surface area [88]. Thermal cracking in asphalt pavements commonly occurs in absolute tensile opening or fracture Mode I. In other words, the cracks grow perpendicular to the direction of the thermal-induced stresses in the pavement, i.e., transverse to the direction of traffic [88]. It is believed that the low-temperature DC(T) test controls not only the first mode of cracking but also accounts for the second mode partially [18]. Several studies have suggested advantages of the DC(T) over other testing procedures in controlling thermal cracking and correlation with field performance [20,23,51,52]. Fracture energy of asphalt mixture is the most important output of the DC(T) test. The performance-based specifications utilize fracture energy as performance parameter because it correlates well with the field cracking performance

* Corresponding author.
E-mail addresses: alavia@missouri.edu, ah_alavi@hotmail.com (A.H. Alavi).

https://doi.org/10.1016/j.measurement.2018.11.081
0263-2241/© 2018 Elsevier Ltd. All rights reserved.

Fig. 1. Typical thermal cracks in a pavement segment located on U.S. Route 63 in Missouri.

[38]. This parameter measures the amount of work required to fracture an asphalt core along a fabricated notch in the specimen [16]. Fig. 2 shows the correlation between observed transverse cracking in asphalt mixtures and their corresponding DC(T) fracture energies based on the data from states of Illinois, Minnesota, Missouri, and Wisconsin [20]. As seen in this figure, fracture energy is strongly correlated with low-temperature cracking.

However, asphalt mixture performance testing is sometimes cost-prohibitive and/or component materials may not be available or known during the pavement thickness design process. Therefore, developing a relationship between the fracture energy measured using the DC(T) test and known or estimated parameters from the asphalt mixture specimen leads to considerable savings in construction cost and time. While there are some prediction models for fracture in bituminous materials [41,46], none of them deals with correlating the asphalt fracture energy from performance tests with component mixture properties.

Based on this motivation, the goal of this study was to develop comprehensive models for predicting the fracture energy of asphalt mixture specimens. To this aim, robust machine learning methods termed gene expression programming (GEP) and hybrid artificial neural network/simulated annealing (ANN/SA) are used to build the prediction models. The machine learning algorithms are calibrated using a set of DC(T) fracture energy data for asphalt mixtures. A key feature of the proposed models is that they include simultaneous effects of various testing, binder and aggregate-related parameters, along with modern asphalt ingredients such as recycled materials, rejuvenators, rubber and their interactions. The derived design equations can be considered as variable tools for routine pre-design practice via spreadsheet programming or hand calculations. The models are further evaluated using some recommended criteria and are benchmarked against one other.

2. Machine learning techniques

In general, a challenging issue for modeling the fracture energy is to find the most suitable factors and simulation techniques. Traditional regression analysis is one of the basic techniques for this purpose. However, structure of a regression model should be defined in advance, which is not always an optimal solution [2]. To deal with this issue, researchers are now widely using machine learning (ML) techniques as powerful empirical regression approaches [44]. ML is a subdivision of artificial intelligence (AI) inspired by biological learning processes. The ML algorithms can learn the underlying behavior of a system from a set of training data without a prior knowledge about the nature of the relationships between the data [59]. ML is a collection of various algorithms such as ANN, support vector machines (SVM), etc. These techniques have proven useful for many civil engineering applications including prediction of asphalt concrete properties (e.g. [7–9,12,15,26–30,36,54,58,62,64,65–67,75–79,81,83,91].

Despite the reliable performance of these techniques, they are considered as black-box tools. That is, they are usually unable to generate practical prediction equations [2]. In addition, the ML techniques and more specifically ANNs are prone to being stuck in local minima [3]. This issue can be tackled by integrating the ANN training process with powerful optimization algorithms such as simulated annealing (SA) [3,13,45,49,68,82]. While a hybrid ANN and SA (ANN/SA) method has a remarkably better prediction performance than standard ANN [3,61], there are not any studies in the area of its application to the characterization of the bituminous material. In this study, the so-called ANN/SA-based black-box system is opened, and the developed model is converted it into a practical design equation. In addition, with the advent of genetic programming (GP) [43], the limitation of the black-box methods

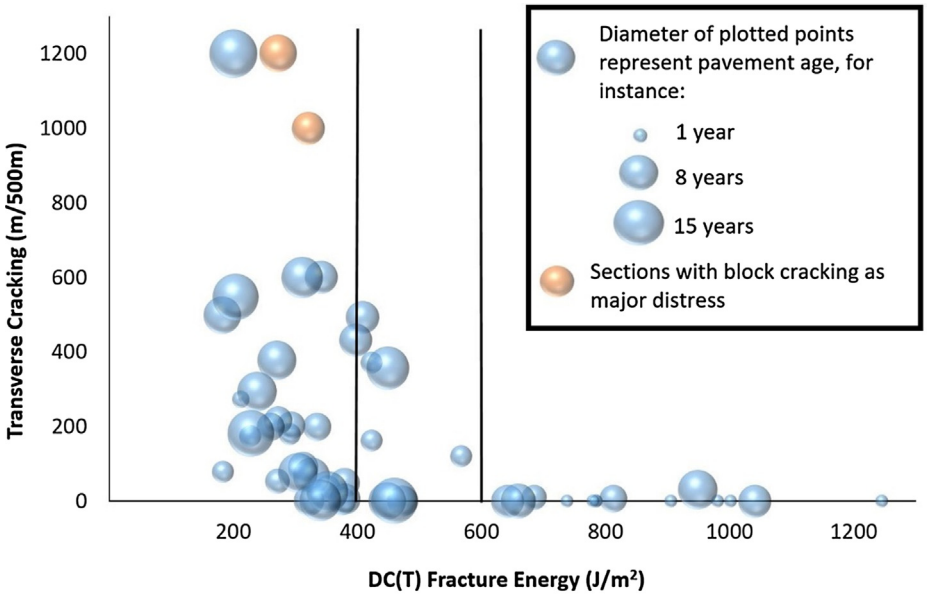

Fig. 2. DC(T) fracture energy vs. transverse cracking [20].

has been tackled. This is because the GP-based methods can generate precise non-linear mathematical models for an investigated system [28,31,39]. The current research is also aimed at deploying one of the robust branches of classical GP called GEP to develop highly nonlinear models for the prediction of fracture energy of asphalt mixtures.

2.1. Gene expression programming

Invented by Koza [43], GP is an extension to genetic algorithm (GA) that can automatically generate mathematical models following the Darwinian evolutionary theory. While the GA solutions are a sequence of numbers, GP creates programs that usually have a tree-shape structure [3]. Three major types of GP are shown in Fig. 3.

GEP is a linear GP method proposed by Ferreira [25]. GEP uses strings with a fixed length of characters to define solutions. The evolved solutions are expressed as Expression Trees (ETs). GEP can evolve complex programs composed of several subprograms [87]. Genes in GEP are a combination of functions or terminal sets [3,4]. An example of genes expressed in Karva notation (KN) is as follows:

$$+.\times.cos.a.-.+.+.\times b.a.c.-4.b.a \quad (1)$$

This KN can be transformed into a tree-shape ET as shown in Fig. 4.

The ET given in Fig. 4 can be expressed in a functional form as:

$$a((c-4)-(b\times a))+cos(b+a) \quad (2)$$

The main steps that GEP follows to obtain a solution can be found in [25]. GEP uses various genetic operators such as crossover, mutation and rotation [71]. In order to reshape the ETs, the rotation operator plays a key role by rotating two parts of a program [3,25]. For instance, Eq. (3) shows how the first five elements of original gene are rotated to create a new program:

$$+.+.\times b.a.c.-4.b.a.+.\times.cos.a.- \quad (3)$$

The above equation can be transformed to $(b+a)+(c\times-4)$, as visualized in Fig. 5. More details about classical GP and GEP can be found in [3,25].

2.2. Hybrid ANN/SA method

ANNs are among the most widely used branches of ML. Fig. 6 shows the basic structure an ANN neuron. In this neuron, a weight coefficient is applied to the inputs and a summation function sums the weighted inputs and bias. The output is then calculated by a transfer function [1,2,74].

One of the concerns during the ANN training process is to find optimal initial weight values [2]. This can be done using robust optimization algorithm such as SA [45]. More details about the basic SA method can be found in [42,57]. A flowchart describing the ANN/SA method is presented in Fig. 7. Boltzmann distribution is used in the SA method to accept the solution improving the performance. The SA-based optimization process is shown in Fig. 8. The parameters involved in the algorithm are configuration of energy ($E(x)$), k is Boltzmann's constant (k), and temperature (T) to define the probability (P_a) of any actual state of x [42,72]. Two cooling schedules in SA are presented in Fig. 9. More details about these schedules and the ANN/SA training process is given in [2,42,72].

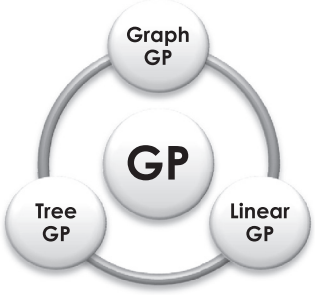

Fig. 3. Different types of GP [3].

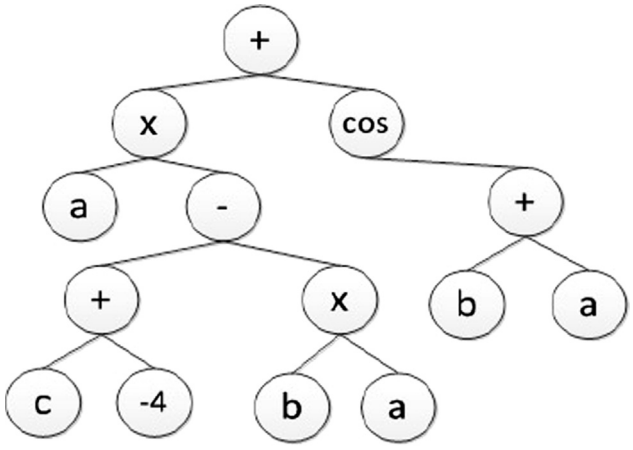

Fig. 4. Translating KN to an ET.

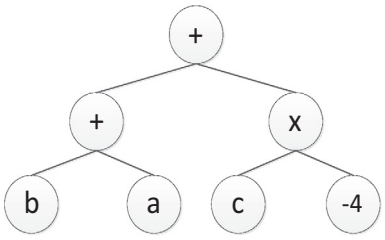

Fig. 5. The rotated ET.

3. Modeling of fracture energy of asphalt concrete

As discussed before, none of the previous studies have taken into account the combined effect of testing, binder, aggregate, and recycling parameters for the prediction of the asphalt concrete fracture energy (G_f). This is unfortunate, since the influence of these parameters on G_f is now fairly well-understood [18]. In this research, the parameters which were believed to affect the low temperature cracking resistance of asphalt concrete in DC(T) test were extracted from relevant literature and are categorized in three groups: testing temperature, aggregate-related parameters, and binder-related parameters.

DC(T) testing temperature: According to the ASTM specification [6], the DC(T) test is performed at 10°warmer than the low temperature performance grade (LTPG) of the binder. As the sample temperature is reduced, the asphalt binder becomes more brittle and its fracture resistance decreases [88,90]. SCB and DC(T) testing temperatures are defined based on the performance grade (PG) of the binder [48]. Statistical analysis showed that testing temperature is a significant parameter to explain the variations of the SCB and DC(T) G_f [48].

Aggregate-related parameters: The aggregates form the skeleton of asphalt pavements. Depending on the required performance,

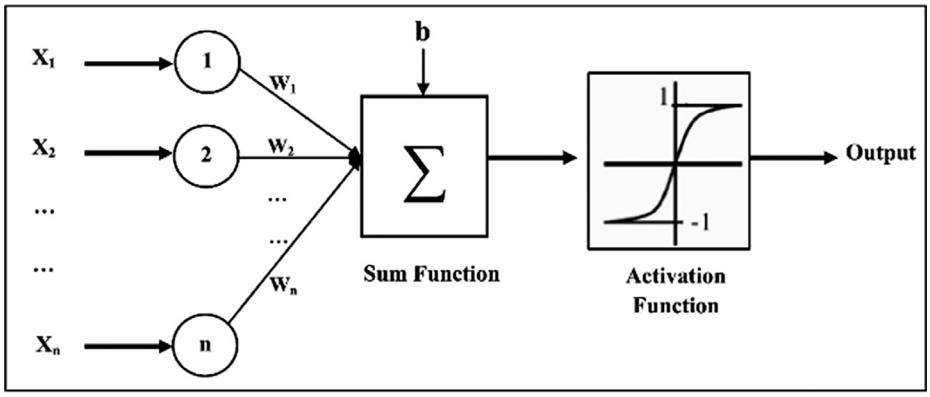

Fig. 6. Basic structure of an ANN neuron [1].

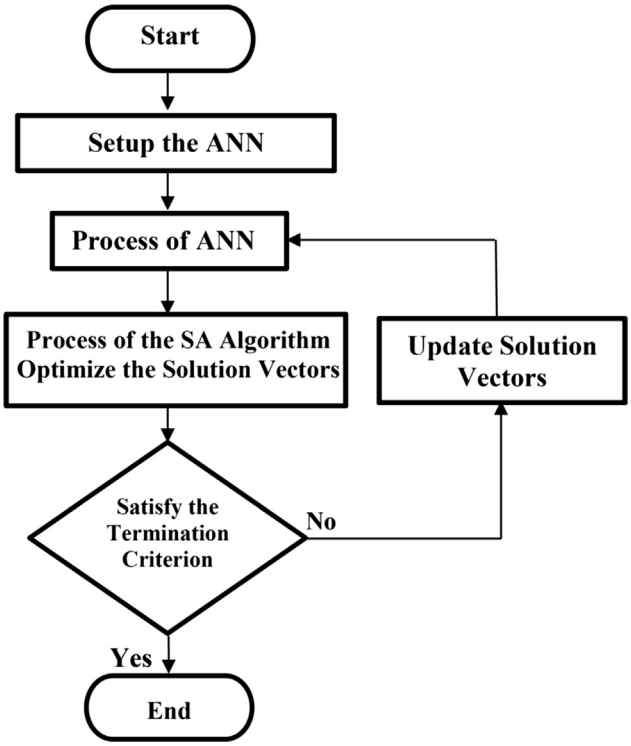

Fig. 7. Flowchart of the ANN/SA method.

The SA Algorithm

Choose at a random initial solution x_0 to be optimized
Initialize the parameters: temperature T, Boltzmann's constant k, reduction factor c
while termination criterion is not satisfied **do**
  for number of new solution
    Select a new solution: $x_0+\Delta x$
      if $E(x_0+\Delta x) > E(x_0)$ **then**
        $E_{new} = E(x_0 + \Delta x)$; $x_0 = x_0 + \Delta x$
        else
          $\Delta E = E(x_0 + \Delta x) - E(x_0)$
          random $r(0, 1)$
            if $r > e^{-\frac{\Delta E}{kT}}$ **then**
              $E_{new} = E(x_0 + \Delta x)$, $x_0 = x_0 + \Delta x$
              else
              $E_{new} = E(x_0)$,
            end if
      end if
    $E = E_{new}$
    Decrease the temperature periodically: $T = c \times T$
  end for
end while

Fig. 8. Pseudo-code for the SA algorithm.

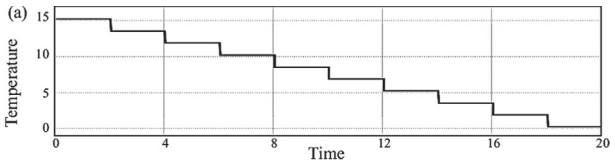

(a) Linear cooling

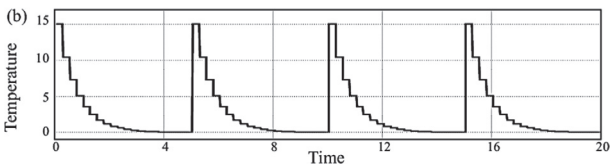

(b) Temperature cycling

Fig. 9. Cooling schedules in SA [2].

dense-graded, gap-graded, and open-graded gradation types are used in asphalt production. Nominal maximum size (NMAS) provides an appropriate means to compare the size range of each gradation type. In addition to the gradation, aggregate type and chemical mineralogy affect the binder-aggregate interaction and the low temperature cracking performance of asphalt mixture. Buttlar et al. [18] observed that mixtures with crushed gravel aggregates outperformed the mixtures with dolomitic limestone in terms of the DC(T) G_f and Hamburg rut depth. Benefiting from more durable aggregates and higher asphalt content, stone matrix asphalt (SMA) exhibited superior fracture resistance comparing to conventional dense-graded hot mix asphalt (HMA) [18]. Also, the mean DC(T) and SCB G_f of granite mixtures was measured to be higher than limestone mixtures [47,48].

Binder-related parameters: Asphalt binder plays and important role in low temperature behavior of asphalt mixture. If properly chosen, the binder can provide the flexibility and ductility needed by asphalt concrete to relax the induced thermal stress. Therefore, a soft binder outperforms a stiff binder in terms of low temperature cracking [18]. In spite of this fact, the soft binder may lead to rutting distress at high climates. As a result, a binder with a

higher range of useful temperature interval (UTI) is desirable to withstand the cracking and rutting at low and high temperatures, respectively. In addition to the neat binder gradation, application of recycled materials such as reclaimed asphalt pavement (RAP) and reclaimed asphalt shingles (RAS), and also additives (e.g. rejuvenator agents, warm mix, styrene-butadienestyrene (SBS), and acids) affect the binder gradations and properties [14,22].

3.1. Recycled materials (RAP and RAS)

Behnia et al. [11] performed DC(T) on asphalt mixtures containing 0, 10, 20, 30, 40 and 50% Asphalt binder replacement (ABR) by RAP. Results showed that addition of RAP consistently decreased the G_f of asphalt samples containing PG58-28 binder. However, mixtures with PG64-22 binder were less sensitive to addition of RAP [11]. Moreover, researchers reported that the mixtures with RAS had lower DC(T) G_f and higher DC(T) peak loads than the control mixture [5].

3.2. Rubber modification

To address the environmental concerns about crumb tire rubber and to improve the performance of asphalt concrete, ground tire rubber (GTR) and engineered crumb rubber (ECR) have attracted considerable attention. An improvement in low temperature performance of asphalt mixture is reported after using these additives in indirect tension (IDT) and asphalt concrete cracking device (ACCD) tests [24]. Also, incorporating ground tire rubber with PG64-28 and PG64-34 led to an improvement in the DC(T) G_f of SMA mixtures at both −12 and −18 °C [17].

3.3. Additives

Polyphosphoric acid (PPA) + SBS and SBS modified mixtures showed higher fracture resistance in DC(T) test than PPA and PPA + Elvaloy modified mixtures [90]. Also, PPA helped mixtures with PG58-28 binder yield higher G_f than those with PG64-28 [60]. The DC(T) test on both the laboratory compacted and field collected samples showed that the crumb rubber warm mix asphalt (CR-WMA) with Evotherm and the CR-HMA exhibited a comparable low temperature performance [89].

Table 1 presents a summary of the parameters included in various studies. On the basis of this literature review, we have developed new models using the GEP and ANN/SA approaches correlating G_f with the influencing variables as follows:

$$G_f = f(UTI,\ LTPG,\ AC,\ NMAS,\ RAP,\ RAS,\ G,\ AT,\ CRC,\ T) \quad (4)$$

Where,

UTI (°C): Useful temperature interval (i.e., for PG 64-22 binder, UTI = 64-(−22) = 86 °C)
LTPG (°C): Low temperature performance grade (for PG 64-22 binder, this is −22 °C)
AC (%): Asphalt content
NMAS (mm): Nominal maximum aggregate size. In this study, NMAS can take 9.5 mm or 12.5 mm.
RAP (%): Reclaimed asphalt pavement
RAS (%): Reclaimed asphalt shingles
G: Gradation type (Dense: 1; SMA: 2; Gap-Graded: 3)
AT: Aggregate type (Limestone: 1; Granite: 2; Gravel: 3)
CRC (%): Crumb rubber content (No additive: 0; 12% GTR: 1; 10% ECR: 2; 10% Evoflex: 3)
T (°C): Testing temperature

It should be noted that the GEP and ANN/SA algorithms are algebraic and cannot take qualitative/categorical data. To tackle this issue, the categorical inputs, i.e. *G*, *AT*, and *CRC*, are transformed into representative numerical codes before the learning algorithms are applied.

3.4. Experimental database

The models are developed using 51 test results obtained from previous studies [16,17,19,37,80] and 6 test results from the current study. The DC(T) tests were performed according to ASTM D7313-07. The testing procedure included conditioning of the fabricated specimen at the selected test temperature in a temperature-controlled chamber for a minimum of two hours. The DC(T) test temperature is generally 10 °C higher than the PG low-temperature grade of the binder used in the asphalt mixture. After the conditioning, the specimens were suspended on loading pins in DC(T) machine, shown in Fig. 10. The specimens were pulled with steel loading dowels through drilled holes, forcing a crack to propagate outward from the notch. The test was carried out at a constant Crack Mouth Opening Displacement (CMOD) rate of 1 mm/min (0.017 mm/s). The test was stopped when the post-peak loading reaches a nominal level of 0.1kN. A typical load-CMOD curve is shown in Fig. 11.

G_f can be obtained by measuring the area under the load-CMOD curve and dividing it by the fractured area (ligament length times thickness) as follows:

$$G_f = \frac{AREA}{B \cdot L} \quad (5)$$

Table 1
A summary of the parameters affecting low-temperature cracking resistance of asphalt concrete in the DC(T) test.

Authors	Variables Investigated
Li et al. [48]	Testing temperature Aggregate source
Buttlar et al. [18]	Aggregate type Aggregate gradation Binder PG grade
Dave et al. [22]	Recycled materials (RAP) Additive
Blankenship and Zeinali [14]	Binder PG grade Polymer and rubber modification
Behnia et al. [11] Dave et al. [22]	Recycled materials (RAP)
Arnold et al. [5]	Recycled materials (RAS)
Buttlar and Rath [17]	Rubber modification
Zegeye et al. [90]	Additive
Mogawer et al. [60]	Additive

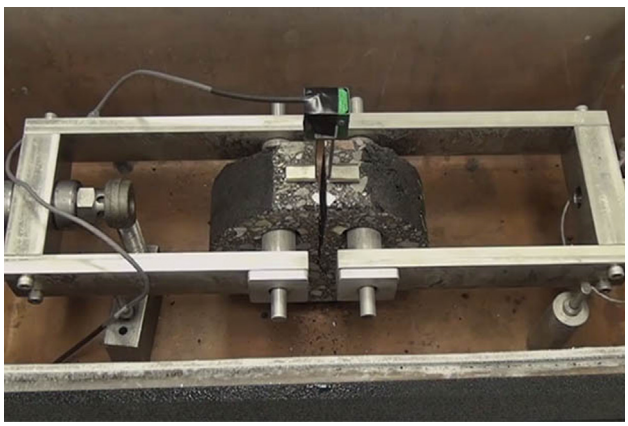

Fig. 10. The test Quip DC(T) apparatus.

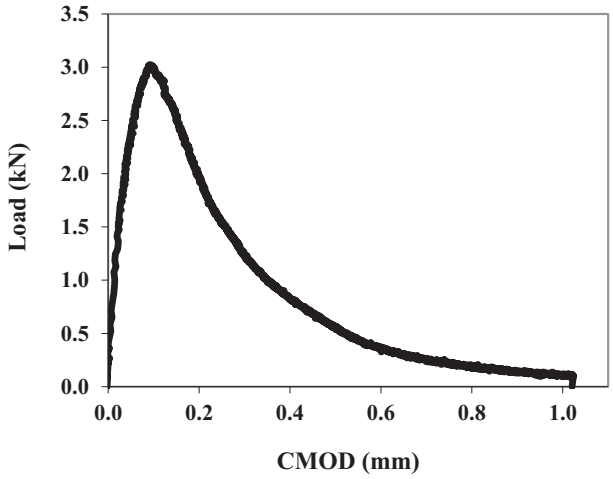

Fig. 11. Typical Load-CMOD curve from DC(T) testing.

where,

G_f = Fracture energy, in J/m^2
AREA = Area under Load-CMOD$_{FIT}$ curve, until the terminal load of 0.1 kN is reached
B = Specimen thickness, in m, generally 0.050 m (except for field cores)
L = Ligament length, usually around 0.083 m

The numerator of the equation represents the area under the Load-CMOD curve, which is the work required to create the fracture surface. The area is generally computed using the quadrangle rule for numerical integration. The CMOD curve is generally the fitted CMOD, where a straight line is fit through the CMOD vs. time curve to enable data smoothing (ASTM D7313-07).

Table 2 presents the descriptive statistics of the variables used in this study. To deal with overfitting, three random divisions were considered for the data: learning (~70%), validation (~10%) and testing (~20%) [9,10,21,63]. The learning and validation subsets were used to calibrate and evaluate the models, respectively. Since they were both involved in selecting the final models, they were labeled as training data in the subsequent analyses. To visualize the distribution of the samples, the data are presented by frequency histograms (see Fig. 12). As observed from Fig. 12, the distributions of the predictor variables are not uniform. Arguably, better model performance is expected for cases within the ranges given in Table 2 and where the densities of the variables are higher as shown in Fig. 12.

3.5. Performance measures

Determination coefficient (R^2), root mean squared error (RMSE) and mean absolute error (MAE) were used as the performance measures:

$$R^2 = \frac{\left(\sum_{i=1}^{n}(O_i-\bar{O}_i)(t_i-\bar{t}_i)\right)^2}{\sum_{1=1}^{n}(O_i-\bar{O}_i)^2\sum_{i=1}^{n}(t_i-\bar{t}_i)^2} \quad (6)$$

$$RMSE = \sqrt{\frac{\sum_{i=1}^{n}(O_i-t_i)^2}{n}} \quad (7)$$

$$MAE = \frac{\sum_{i=1}^{n}|O_i-t_i|}{n} \quad (8)$$

where,

O_i : Measured output
t_i : Predicted output
$\bar{O}_i$: Average of measured outputs
$\bar{t}_i$: Average of predicted outputs
n: Number of samples

The best GEP models were selected based on a multi-objective strategy that involved simplicity of the models and their least prediction error during the learning and validation stages [9].

3.6. Model development using the GEP method

After a series of preliminary runs and observing the GEP algorithm performance, *UTI*, *LTPG*, *AC*, *NMAS*, *RAP*, *RAS*, *G*, *AT*, *CRC*, and *T* were determined to be the most influencing parameters. Then, the GEP method was used to arrive at the best mathematical models. Several runs were carried out to determine the optimized GEP parameters. There are five main parts for setting GEP parameters including: general setting, complexity increase, genetic operators, numerical constant, and fitness function. In general part, number of chromosomes affects the time of the simulation run. By increasing the number of chromosomes, the runs take longer. The head size shows the complexity of each term in the evolved model [3,4,61]. Table 3 shows a set of parameters used during the GEP simulations.

The overall number of runs for developing the optimal models was about 54 (number of combinations of the algorithm parameters) × 3 (number of replications) = 162. The optimal GEP-based prediction model for G_f is as follows:

$$\begin{aligned} G_f\left(\frac{j}{m^2}\right) = {} & ((((NMAS-9)AT-RAP)(5.36+T-LTPG))-LTPG) \\ & + AT\left(G^4-1.7+UTI\right)+\frac{NMAS-UTI}{((T+NMAS)AT)-AT+6.45} \\ & - RAS+RAP+\frac{LTPG}{AT}+LTPG^2+3.49T+AC\times RAP \\ & + T\sqrt{CRC^3-10T-RAP\times AC-6.461+UTI} \end{aligned} \quad (9)$$

where, *UTI*, *LTPG*, *AC*, *NMAS*, *RAP*, *RAS*, *G*, *AT*, *CRC*, and *T* denote useful temperature interval, low temperature performance grade, percentage of asphalt content, nominal maximum aggregate size, percentage of reclaimed asphalt pavement, percentage of reclaimed asphalt

Table 2
Descriptive statistics of the variables.

Parameter	*UTI* (°C)	*LTPG* (°C)	*AC* (%)	*NMAS* (mm)	*RAP* (%)	*RAS* (%)	*G*	*AT*	*CRC*	*T* (°C)	G_f (j/m^2)
Mean	88.35	−29.37	6.14	–	5.41	8.81	–	–	–	−17.37	710.64
Median	86.00	−28.00	6.00	–	0.00	0.00	–	–	–	−12.00	658.00
Mode	86.00	−28.00	6.00	–	0.00	0.00	–	–	–	−12.00	590.00
Kurtosis	−0.43	−0.68	0.27	–	3.70	−0.90	–	–	–	2.66	10.83
Skewness	−0.09	−0.27	−0.03	–	1.89	0.93	–	–	–	−1.75	2.78
Range	28.00	18.00	2.30	–	35.20	33.50	–	–	–	30.00	2434.70
Minimum	70.00	−40.00	5.10	9.50	0.00	0.00	1	1	0	−42.00	283.00
Maximum	98.00	−22.00	7.40	12.50	35.20	33.50	3	3	3	−12.00	2717.70

shingles, gradation type, aggregate type, crumb rubber content, and testing temperature, respectively. The model is a complicated combination of parameters and operators to predict G_f. The expression trees (ETs) of the obtained model is given in Fig. 13. In this figure, d0, . . ., d9 represent *UTI*, *LTPG*, *AC*, *NMAS*, *RAP*, *RAS*, *G*, *AT*, *CRC*, and *T*, respectively. Parameters c_0 and c_1 in the ETs are numerical constants, n in Xn denotes power. This model is comprised of five individual sub-models connected using addition operation. Each of

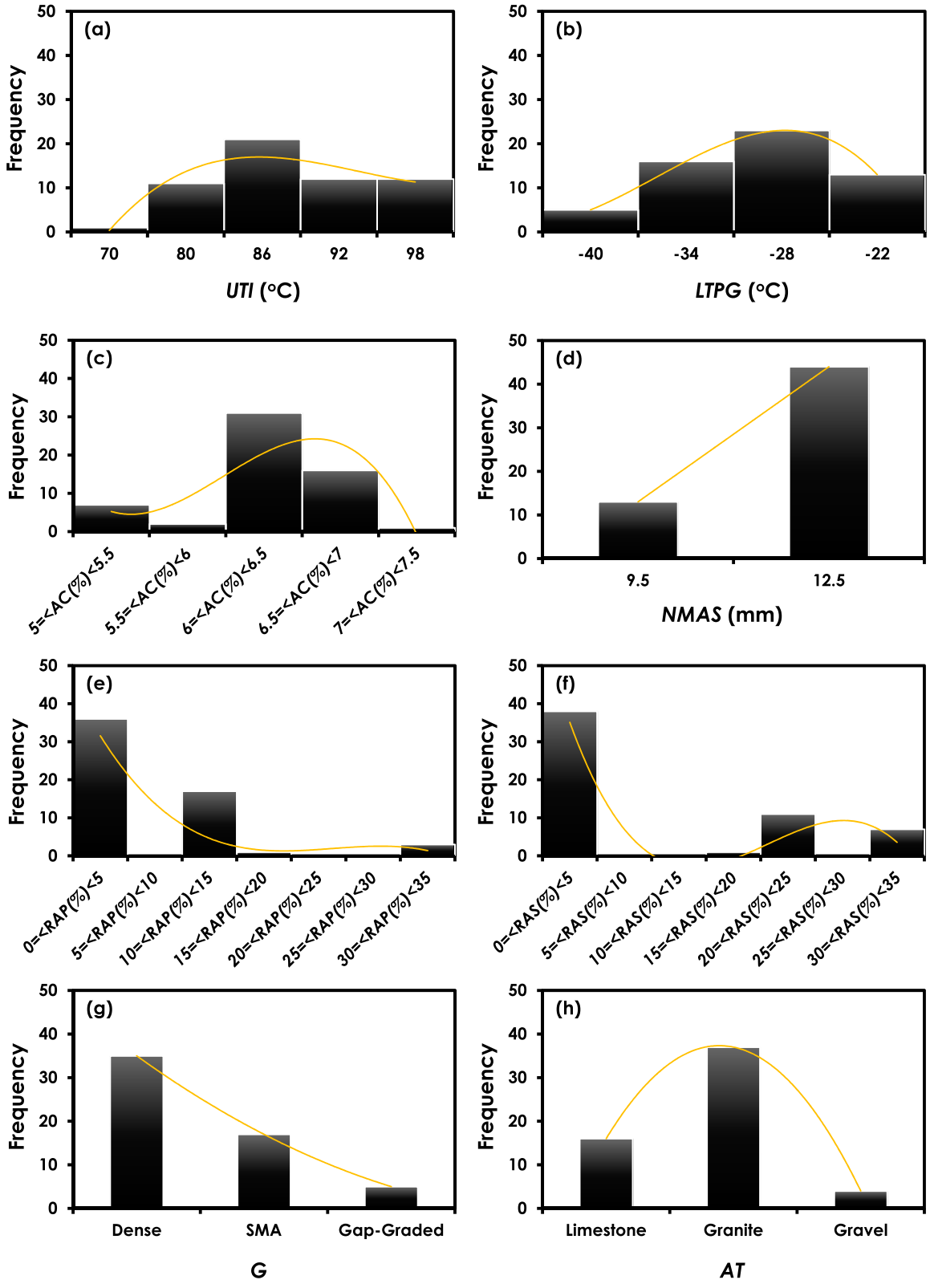

Fig. 12. Distribution histograms of the variables.

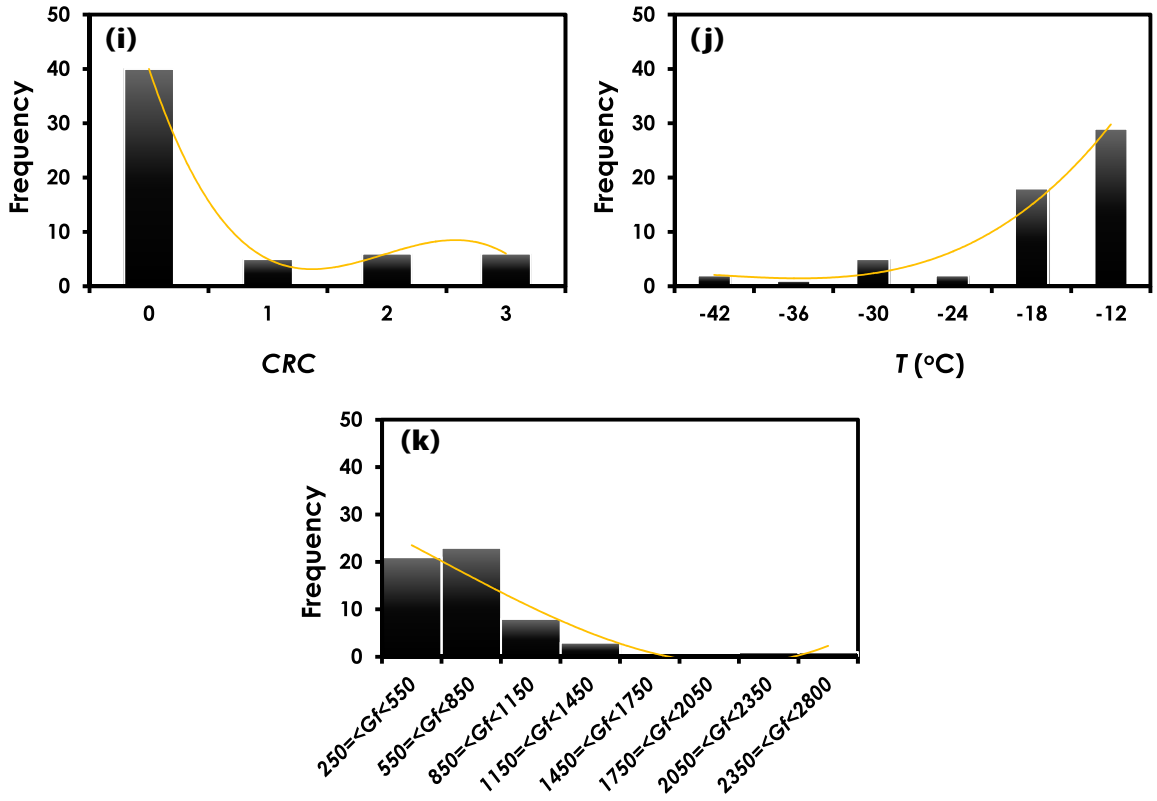

Fig. 12 (*continued*)

Table 3
The optimal parameter setting for the GEP algorithm.

Parameter	Settings
General	
Chromosomes	20, 30, 50
Genes	3, 4, 5
Head size	8, 10, 15
Linking function	Addition
Function set	+, −, ×, /, $\sqrt{}$, $\sqrt[3]{}$, Ln, Log, power, exp
Complexity increase	
Generations without change	2000
Number of tries	3
Max. complexity	5
Genetic operators	
Mutation rate	0.00138, 0.044
Inversion rate	0.00546
Numerical constants	
Data type	Floating-point
Lower bound	−10
Upper bound	+10

these sub-models include a part of the information provided by the final model [25]. Fig. 14 presents the predictions provided by this model. The high density of the points around the ideal 45-degree angle line clearly indicates the good performance of the model.

3.7. Model development using the hybrid ANN/SA method

The ANN/SA models formulate G_f in terms of *UTI*, *LTPG*, *AC*, *NMAS*, *RAP*, *RAS*, *G*, *AT*, *CRC*, and *T*. For the ANN simulation, the data was normalized between 0.05 and 0.95 using the following method [69,86]:

$$V_n = A \times V + B \tag{10}$$

where,

$$A = \frac{L - U}{V_{max} - V_{min}} \tag{11}$$

$$B = L - A \times V_{max} \tag{12}$$

V_{max} and V_{min} are the maximum and minimum of the variable V in the database, respectively. In this study, L and U were taken 0.05 and 0.95, respectively. The normalized data were then fed into the ANN/SA algorithm. The algorithm was implemented several times to find the best solution. The ANN/SA parameter setting was based on some previously suggested values [2,45] and after a trial-and-error approach. The best ANN/SA simulation results were obtained with these parameter values: $k = 1500$; initial temperature = 15; final temperature = 0.015. The number of temperature cycles were set to 10, 20 and 50. Also, 10, 15 or 20 iterations were considered for the number of iterations. Several networks with different settings for hidden layers, hidden nodes, epochs, and activation functions were trained. Conjugate-Gradient and Levenberg–Marquardt algorithms were implemented for the training of the network. The best results were obtained by the Conjugate-Gradient method. Also, the transfer function between the input and hidden layer was log-sigmoid of form $1/(1 + e^{-x})$. The same function was used for the hidden layer and output layer.

In order to transform the ANN/SA model into a practical equation, the weights and biases were frozen after the networks were well trained [2]. Thereafter, the optimal model was converted to a functional form using the following equation [2,34]:

$$h = f_{HO}\left(bias_h + \sum_{k=1}^{h} V_k f_{IH}\left(bias_{hk} + \sum_{i=1}^{m} w_{ik} x_i\right)\right) \tag{13}$$

where h, $bias$, V, w, x, and f denote output, bias, weight connection, input, and transfer function, respectively. Also, h, IH, HO, k, i represent the hidden layer, input-hidden layer, hidden-ouput layer, number of

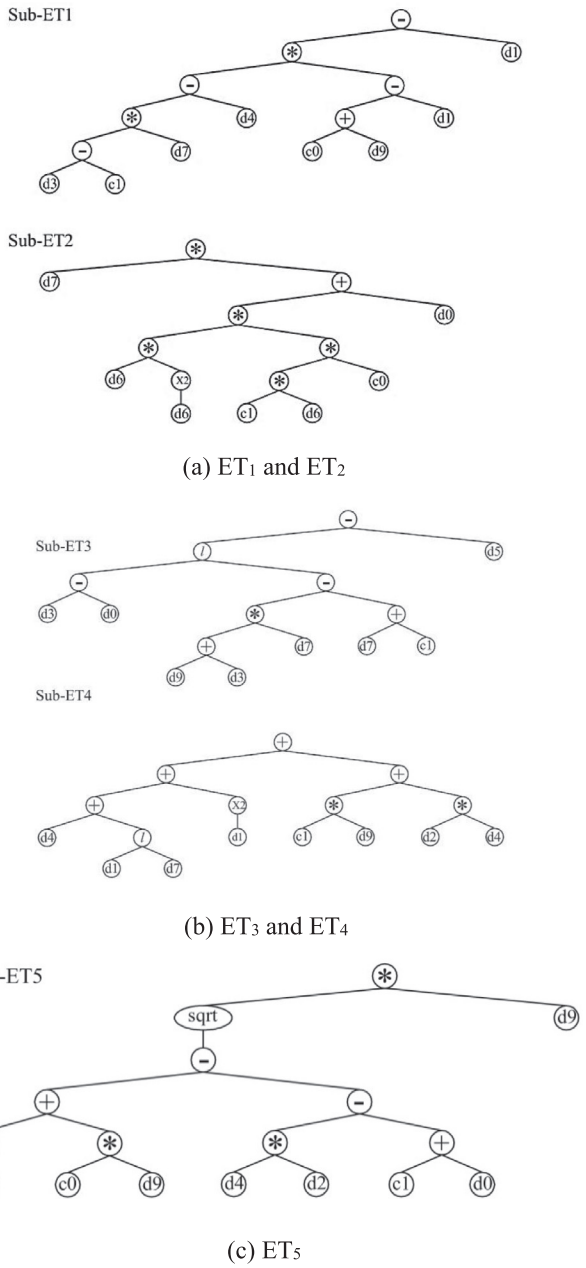

Fig. 13. Expression trees of the best GEP prediction model for G_f (ET = $\sum$Sub-ET$_i$).

neurons, and number of input parameter, respectively. The best ANN/SA prediction model for G_f was constructed with all of the 10 input parameters (*UTI*, *LTPG*, *AC*, *NMAS*, *RAP*, *RAS*, *G*, *AT*, *CRC*, and *T*) and 11 (m = 11) nodes (see Fig. 15). After de-normalizing the output, the ANN/SA-based formulations of G_f is as follows:

$$G_f(j/m^2) = -2705.22\left(\frac{1}{1+e^{-(A+Bias_h)}}\right) + 2852.97 \tag{14}$$

where,

$$A = \sum_{k=1}^{11} \frac{V_k}{1+e^{-F}} \tag{15}$$

$$F = UTI_nW_{1k} + LTPG_nW_{2k} + AC_nW_{3k} + NMAS_nW_{4k} + RAP_nW_{5k} + RAS_nW_{6k} + G_nW_{7k} + AT_nW_{8k} + CRC_nW_{9k} + T_nW_{10k} + Bias_k \tag{16}$$

in which, UTI_n, $LTPG_n$, AC_n, $NMAS_n$, RAP_n, RAS_n, G_n, AT_n, CRC_n, and T_n represent the inputs variables normalized using Eq. (11). The weight and bias values of the optimal ANN/SA model are given in Tables 4 and 5. 8,000 epochs were considered for the network training. Fig. 16 presents the predicted against the measured G_f values. As seen in this figure, the points are densely distributed around the idea fit line which indicates that the prediction is well-performed.

3.7.1. Design example

The ANN/SA structure interpretation procedure was shown using the following illustrative example for one of the testing data:

UTI = 98 °C; *LTPG* = −40 °C; *AC* = 6.5%; *NAMS* = 12.5 mm; *RAP* = 0%; *RAS* = 0%; *G* = 1 (Dense); *AT* = 2 (Granite); *CRC* = 0%; *T* = −42 °C. G_f is required. Here are the calculation steps:

1: Normalization of the input parameters and calculating UTI_n, $LTPG_n$, AC_n, $NMAS_n$, RAP_n, RAS_n, G_n, AT_n, CRC_n, and T_n based on Eqs. (10)–(12).

For *UTI*: Minimum and maximum are 70 and 98 °C, respectively. Hence:

$$a = \frac{(0.05-0.95)}{(98-70)} = -0.032,\ b = 0.05 - (-0.032)\times 98 = 3.186$$

$$UTI_n = \overbrace{-0.032}^{a} \times \overbrace{98}^{UTI} + \overbrace{3.186}^{b} = 0.05$$

Similarly,

$LTPG_n$, AC_n, $NMAS_n$, RAP_n, RAS_n, G_n, AT_n, CRC_n, and T_n are equal to 0.95, 0.40, 0.05, 0.95, 0.95, 0.95, 0.50, 0.95, and 0.95.

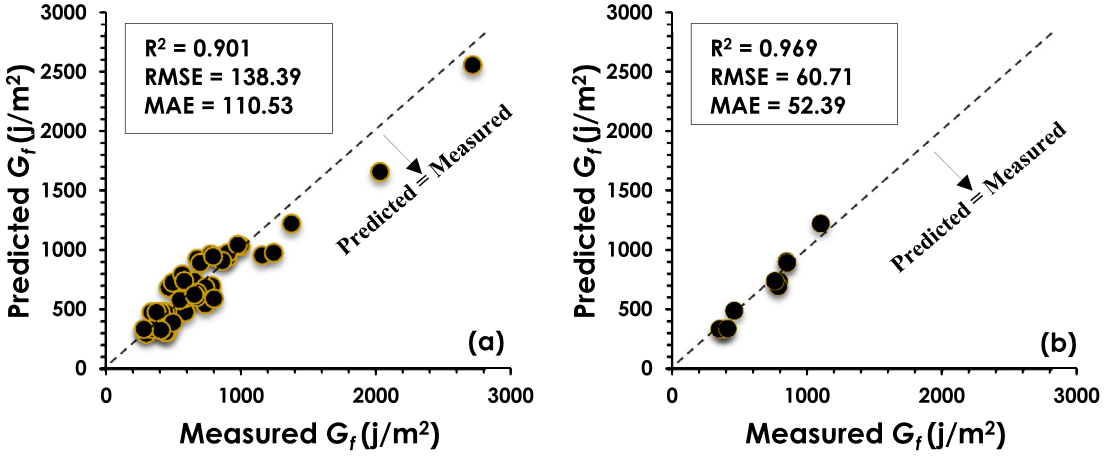

Fig. 14. Measured against predicted G_f using the GEP model: (a) training data, (b) testing data.

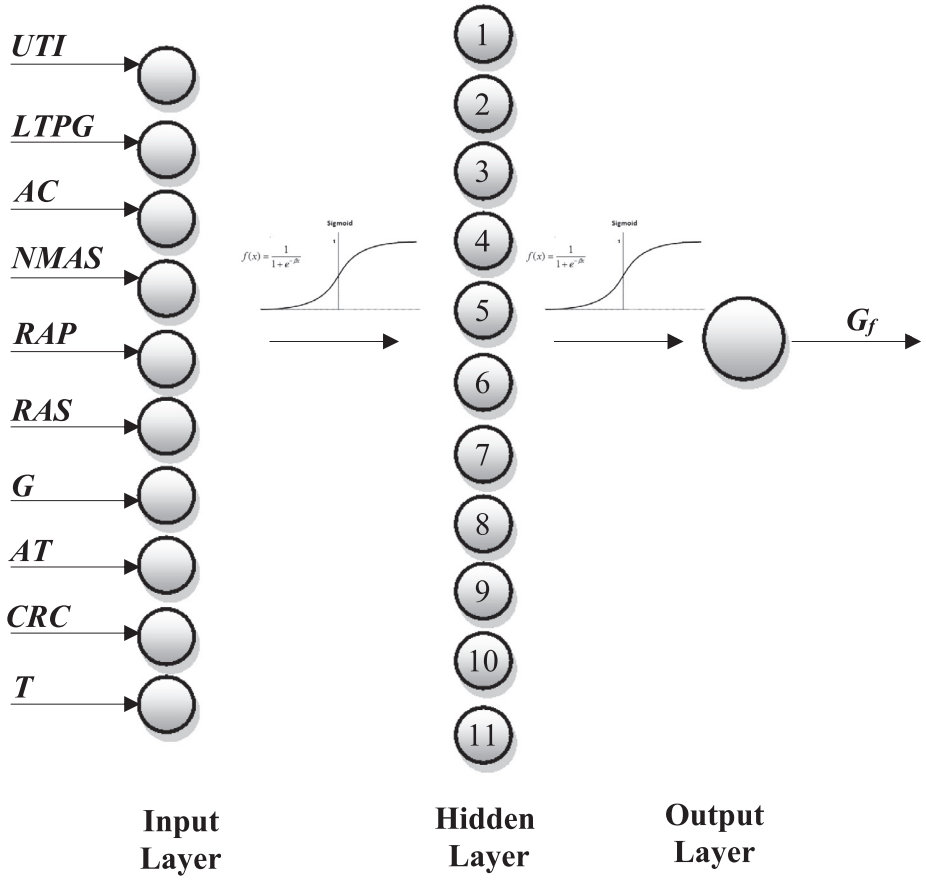

Fig. 15. The optimal ANN/SA architecture for predicting G_f.

Table 4
Input-hidden layer weight and bias values.

Weights	K										
	1	2	3	4	5	6	7	8	9	10	11
W_{1k}	2.080	2.433	−2.212	−2.367	2.501	3.292	2.783	0.072	−0.856	−2.108	3.648
W_{2k}	−6.347	2.589	7.572	4.444	2.218	1.010	−1.156	−0.746	0.025	0.722	3.290
W_{3k}	−9.186	−8.646	−2.193	−3.982	3.947	−1.383	2.968	−6.359	2.101	−0.897	−1.458
W_{4k}	1.552	4.077	5.969	4.724	−4.697	−2.913	3.362	−1.464	2.480	2.120	−5.404
W_{5k}	−2.453	−2.202	1.278	0.836	0.999	−4.285	−0.533	−2.276	−1.258	−2.856	−0.196
W_{6k}	1.694	3.175	−2.713	−0.825	2.747	−6.244	−2.981	−3.682	−1.960	−2.543	−1.345
W_{7k}	0.243	3.847	−1.600	−1.391	−4.705	1.433	1.045	1.030	2.154	−3.012	−0.440
W_{8k}	7.694	−2.359	−0.479	−5.490	9.166	−0.989	2.789	6.021	1.449	−3.242	1.350
W_{9k}	−0.718	5.610	−4.090	1.653	−0.862	−4.424	3.739	1.196	−8.570	−0.276	−0.332
W_{10k}	1.793	−10.472	−2.509	4.828	5.322	0.550	−1.087	5.262	1.105	3.746	4.012
$Bias_k$	−1.789	−5.773	3.986	0.791	−1.905	0.183	1.181	−3.953	5.056	−4.795	0.252

Table 5
Hidden-Output layer weight and bias values.

Weights	K											
	1	2	3	4	5	6	7	8	9	10	11	$Bias_h$
V_k	6.964	−9.361	−2.696	2.694	−5.021	1.550	5.092	3.908	3.591	−14.999	−5.085	4.576

2: Calculation of the hidden layer. Referring to Eq. (16), F_1, …, F_{11} are obtained as:

$F_1 = -6.954$, $F_2 = -7.684$, $F_3 = 1.093$, $F_4 = 5.632$, $F_5 = 9.589$, $F_6 = -12.211$, $F_7 = 3.152$, $F_8 = -2.825$, $F_9 = -1.370$, $F_{10} = -10.785$, and $F_{11} = 4.991$.

3: Predicting G_f. The log-sigmoid function ($f = 1/(1 + e^{-x})$) was used to calculate A:

$$A = 6.964f(F_1) - 9.361f(F_2) + 2.696f(F_3) + 2.694f(F_4) - 5.021f(F_5) + 1.550f(F_6) + 5.092f(F_7) + 3.908f(F_8) + 3.591f(F_9) - 14.999f(F_{10}) - 5.085f(F_{11}) = 0.027$$

Using Eq. (14), G_f is equal to:

$$G_f = -2705.22\left(\frac{1}{1+e^{-(0.027+4.576)}}\right) + 2852.97 = 874.03 \text{j/m}^2$$

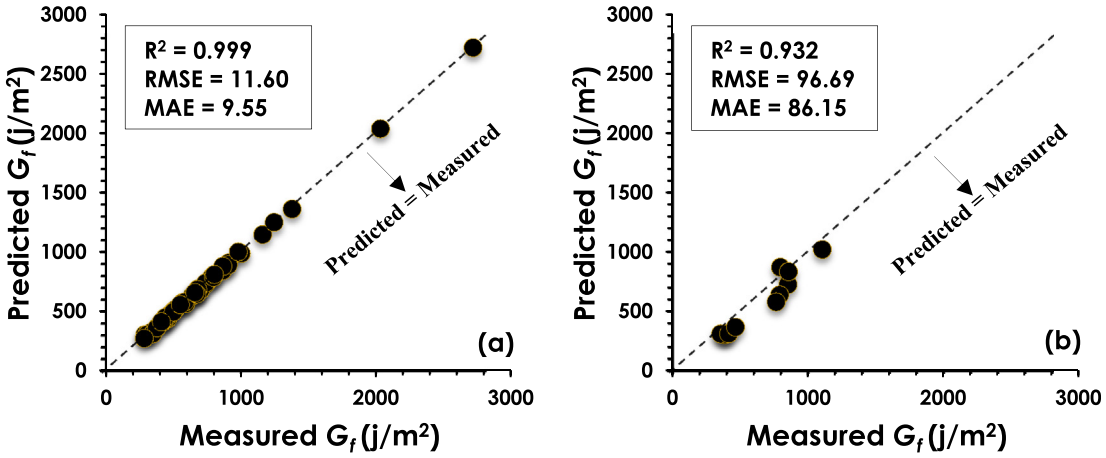

Fig. 16. Measured against predicted G_f using the ANN/SA model: (a) training data, (b) testing data.

The measured G_f for this case was 790.2 j/m^2 which is 11% lower than the predicted G_f .

4. Performance evaluation

4.1. Statistical methods for external validation

On the basis of a rational hypothesis, Smith [84] argues that for correlation coefficient (|R|) higher than 0.8, a strong correlation exists between the predicted and measured values. In all conditions, the error values (e.g. RMSE, MAE) should be at the minimum [4]. Based on the results shown in Figs. 14 and 16, the proposed GEP and ANN/SA models have a satisfactory performance on the training and testing data sets. Besides, Table 6 shows some criteria suggested by Golbraikh and Tropsha [35] and Roy and Roy [73] for the external validation of the models. More details about these performance measures can be found in [26]. As observed from Table 6, the developed models satisfy all of the requisite conditions. The validation phase ensures that the proposed models are strongly suitable and applicable.

4.2. Sensitivity analysis

As discusses in Section 3.3, an extensive simulation study was carried out to find the most relevant parameters and accordingly developing the best predictive models. The optimal models were built using 10 input parameters (*UTI*, *LTPG*, *AC*, *NMAS*, *RAP*, *RAS*, *G*, *AT*, *CRC*, and *T*). However, a second phase of sensitivity analysis was further performed to distinguish the parameters with higher contributions in the final models. To this aim, the frequency values [26] of the input parameters were obtained for the GEP models. In case a design variable has appeared in 100% of the best thirty GEP programs, its frequency value will be equal to 1 [26]. For the ANN/SA analysis, Garson's algorithm [32] was utilized to find the relative importance of the predictor variables based on the weights of the ANN/SA model (Fig. 17). Fig. 18 shows the sensitivity analysis results for the GEP and ANN/SA models. For both GEP and ANN/SA, G_f is more sensitive to *AC* and *AT*. Also, the influence of *LTPG* and *T* is high in the GEP analysis. As seen in Fig. 18, the effect of *UTI*, *RAP* and *RAS* on G_f is less than the other parameters. These are expected outcomes because at low temperature, the fracture phenomenon significantly relies on the aggregate type. In this case, cracks propagate through the aggregates and try to break them up and grow. Asphalt binder is the weak component in asphalt mixtures. A soft binder has a better performance compared to a stiff binder in terms of low temperature cracking [18,40]. Lower LTPG will provide higher ductility and flexibility at low temperature, while higher LTPG leads to brittle behavior of binder [50]. In addition, the fracture energy is dissipated significantly near the glass transition temperature [85]. Binders with lower LTPG have lower glass transition temperature. The significantly high effect of temperature on G_f is also reported in different studies [48].

4.3. Comparative study

Since there were not any existing models for the G_f of asphalt pavements, the GEP and ANN/SA were benchmarked against each other. Referring to Figs. 14 and 16, the ANN/SA model has a notably

Table 6
Performance measures for further validation of the GEP and ANN/SA models.

Item	Formula	Condition	GEP	ANN/SA
1	R	$0.8 < R$	0.984	0.965
2	$k = \frac{\sum_{i=1}^{n}(h_i \times t_i)}{h_i^2}$	$0.85 < k < 1.15$	0.981	1.093
3	$k' = \frac{\sum_{i=1}^{n}(h_i \times t_i)}{t_i^2}$	$0.85 < k' < 1.15$	1.011	0.904
4	$m = \frac{R^2 - R_o^2}{R^2}$	$\|m\| < 0.1$	−0.030	0.000
5	$n = \frac{R^2 - R_{o'}^2}{R^2}$	$\|n\| < 0.1$	−0.032	−0.012
6	$R_m = R^2 \times \left(1 - \sqrt{\left\|R^2 - R_o^2\right\|}\right)$	$0.5 < R_m$	0.804	0.918
7	$R_o^2 = 1 - \frac{\sum_{i=1}^{n}(t_i - h_i^o)^2}{\sum_{i=1}^{n}(t_i - \bar{t}_i)^2}, h_i^o = k \times t_i$	Should be close to 1	0.997	0.932
8	$R_{o'}^2 = 1 - \frac{\sum_{i=1}^{n}(h_i - t_i^o)^2}{\sum_{i=1}^{n}(h_i - \bar{h}_i)^2}, t_i^o = k' \times h_i$	Should be close to 1	0.999	0.943

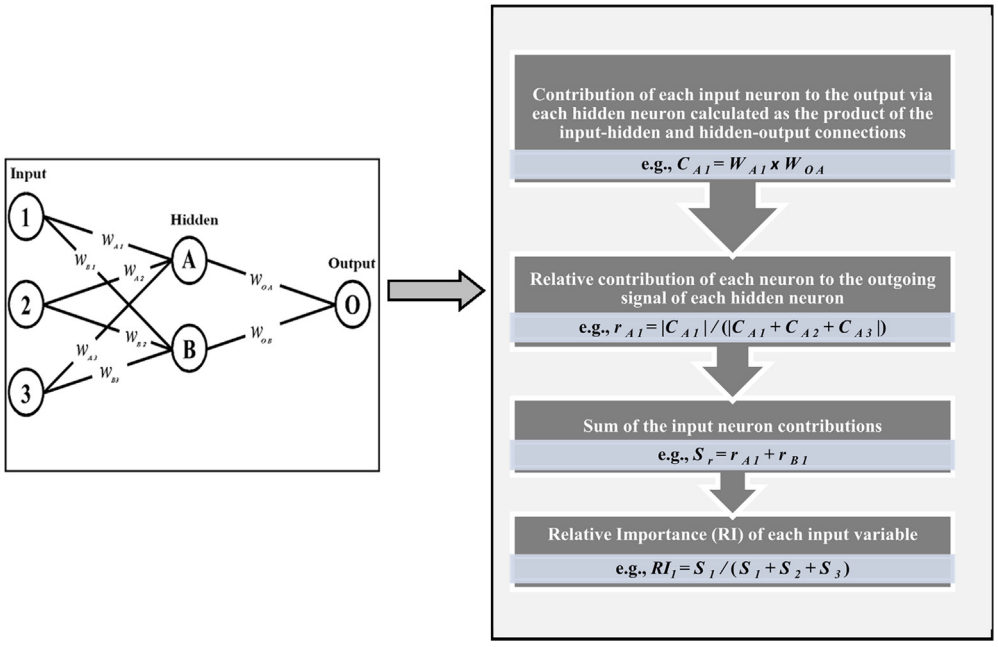

Fig. 17. The procedure to evaluate the relative importance of inputs [32].

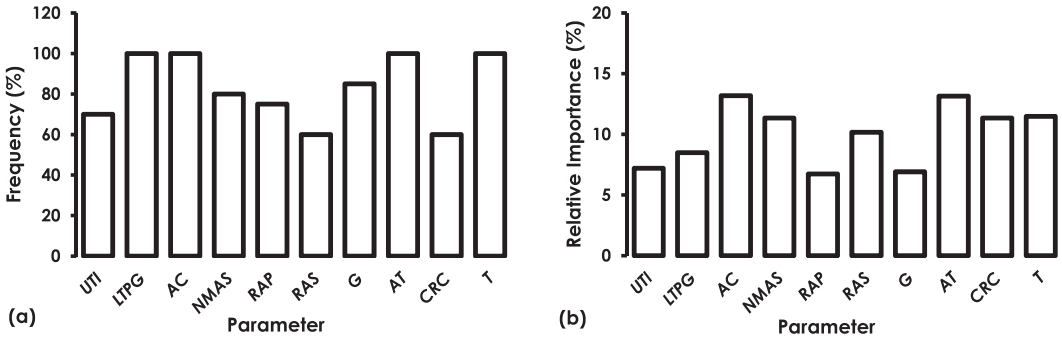

Fig. 18. Sensitivity analysis of the final predictor variables in: (a) GEP analysis and (b) ANN/SA analysis.

better performance than the GEP model on the training data. This is while GEP has a superior performance to ANN/SA on the testing data. This means that the GEP model has a better generalization compared to the ANN/SA model. In addition, Fig. 19 visualizes histogram plots of measured/predicted G_f values along with the standard deviation (STD) and average (Mean) metrics for the entire database. Evidently, the models with higher distribution around Measured G_f/Predicted $G_f = 1$ provide better predictions. As seen in Fig. 19(b), the density of the data corresponding to ANN/SA are higher around 1 compared to the GEP model. On the other hand, GEP provides a better Mean value than the ANN/SA model. It should be noted that a major advantage of GEP over ANN-based and other classical modeling approaches lies in its capability to derive explicit relationships without assuming prior forms of the existing relationships. In addition, the final modes developed using GEP are obtained after controlling millions of nonlinear models, which is not feasible via other nonlinear regression approaches. While this study has opened the black-box ANN/SA model, the derive prediction equation is much more complicated than the GEP model.

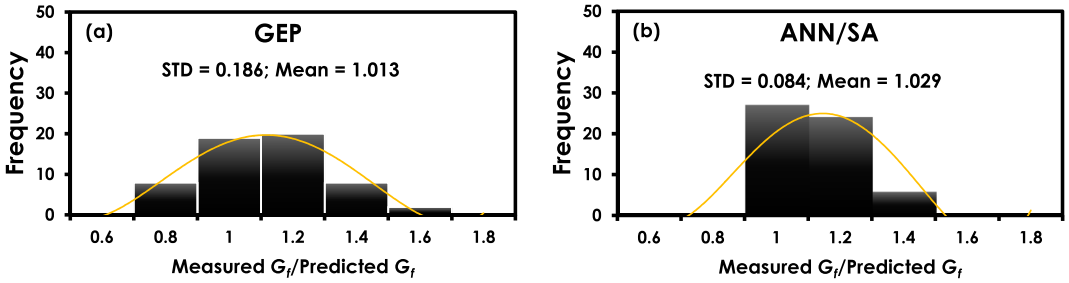

Fig. 19. A comparison of the GEP and ANN/SA models on the entire database.

5. Conclusions

In this study, two machine learning methods called GEP and ANN/SA were used to predict the G_f of asphalt mixtures. Two models were developed using a well-established experimental database. The proposed models include the simultaneous effect of various test, binder and aggregate-related parameters, as well as modern asphalt ingredients such as recycled materials, rejuvenators, and rubber. The models provide reliable predictions of G_f. The GEP model produces better outcomes than the ANN/SA model for the testing data. The beauty of the GEP analysis is that it can model the G_f behavior without any need to predefine the model's functional structure. Besides, a calculation procedure was proposed to transform the optimal ANN/SA model into a functional representation. The GEP model seems to be more practical than the ANN/SA model because of its better generalization and simpler functional structure. However, a limitation of the derived models is that they were calibrated using a fairly limited set of DC(T) test results. This limitation can be overcome by updating the model, allowing to continue to learn (i.e., to grow in predictive accuracy, and eventually mature into a stable and widely predictive tool), as more data becomes available. The results of the sensitivity analysis indicate that *AC*, *AT*, *LTPG* and *T* are more effective to explain the variations of G_f compared with the other predictor variables. Since the proposed models are based on the data alone, they are mostly suitable for pre-design purposes. In any case, the range of the mixture properties should fall within the range considered for the development of the models. In other words, model extrapolation has not been tested and is not recommended at this time. Besides, prior knowledge about the underlying physical process based on engineering judgement or human expertise can also be incorporated into the learning formulation, which greatly enhances the usefulness of GEP over other classical and ML techniques. It should be noted that performing DC(T) test might be cost-prohibitive for some users. Thus, a trial method to design a mixture with acceptable thermal cracking performance may be expensive. Arguably, using the proposed empirical models for the estimation of the DC(T) test results will save time and money for such design procedures.

Further research can focus on including DC(T) test results for mixtures with much wider range properties to obtain more reliable predictions. Moreover, an ML model can be developed to characterize the combined effect of asphalt additives on both rutting and thermal cracking performance. The importance of such model is that adding an additive to asphalt pavement usually improves merely one of these two performance indexes. In addition, a relationship can be developed between the density of the thermal and block cracks in pavement segments and the corresponding DC(T) fracture energy. Further extension of the techniques could eventually allow general pavement distress and performance prediction as a function of traffic and climate for the purposes of general pavement management, material selection, and preliminary mix design.

References

[1] A.H. Alavi, A.H. Gandomi, A. Mollahasani, A.A.R. Heshmati, A. Rashed, Modeling of maximum dry density and optimum moisture content of stabilized soil using artificial neural networks, J. Plant Nutr. Soil Sci. 173 (3) (2010) 368–379.

[2] A.H. Alavi, A.H. Gandomi, Prediction of principal ground-motion parameters using a hybrid method coupling artificial neural networks and simulated annealing, Comput. Struct. 89 (23–24) (2011) 2176–2194.

[3] A.H. Alavi, A.H. Gandomi, A robust data mining approach for formulation of geotechnical engineering systems, Eng. Comput. 28 (2011) 242–274.

[4] A.H. Alavi, A.H. Gandomi, H.C. Nejad, A. Mollahasani, A. Rashed, Design equations for prediction of pressuremeter soil deformation moduli utilizing expression programming systems, Neural Comput. Appl. 23 (2013) 1771–1786.

[5] J.W. Arnold, B. Behnia, M.E. McGovern, B. Hill, W.G. Buttlar, H. Reis, Quantitative evaluation of low-temperature performance of sustainable asphalt pavements containing recycled asphalt shingles (RAS), Constr. Build. Mater. 58 (2014).

[6] ASTM D7313. Standard Test Method for Determining Fracture Energy of Asphalt-Aggregate Mixtures Using the Disk-Shaped Compact Tension Geometry. 2013.

[7] H.M. Azamathulla, A.A. Ghani, S.Y. Fei, ANFIS-based approach for predicting sediment transport in clean sewer, Appl. Soft Comput. 12 (3) (2012) 1227–1230.

[8] H.M. Azamathulla, F.C. Wu, Support vector machine approach for longitudinal dispersion coefficients in natural streams, Appl. Soft Comput. 11 (2) (2011) 2902–2905.

[9] S.K. Babanajad, A.H. Gandomi, A.H. Alavi, New prediction models for concrete ultimate strength under true-triaxial stress states: an evolutionary approach, Adv. Eng. Softw. 110 (2017) 55–68.

[10] W. Banzhaf, P. Nordin, R. Keller, F. Francone, Genetic Programming: An Introduction on the Automatic Evolution of Computer Programs and its Application, Morgan Kaufmann, 1998.

[11] B. Behnia, E. Dave, S. Ahmed, W.G. Buttlar, H. Reis, Effects of recycled asphalt pavement amounts on low-temperature cracking performance of asphalt mixtures using acoustic emissions, Transp. Res. Rec.: J. Transp. Res. Board 2208 (2011) 64–71, https://doi.org/10.3141/2208-09.

[12] A. Behnood, E.M. Golafshani, Predicting the compressive strength of silica fume concrete using hybrid artificial neural network with multi-objective grey wolves, J. Cleaner Prod. 202 (2018) 54–64.

[13] J.M. Binner, K. Graham, A. Gazely, Co-evolving neural networks with evolutionary strategies. A new application to Divisia money, Adv. Econometrics 19 (2004) 127–143.

[14] P.B. Blankenship, A. Zeinali, Evaluation of the DC(T) Test in discerning the variations in cracking properties of asphalt mixtures, Road Mater. Pavement Des. 18 (suppl. 1) (2017) 426–449, https://doi.org/10.1080/14680629.2016.1266772.

[15] A. Bolourchi, S.F. Masri, O.J. Aldraihem, Development and application of computational intelligence approaches for the identification of complex nonlinear systems, Nonlinear Dyn. 79765–786 (2015).

[16] A. Braham, W.G. Buttlar, M. Marasteanu, Marasteanu effect of binder type, aggregate, and mixture composition on fracture energy of hot-mix asphalt in cold climates, Transp. Res. Record: J. Transp. Res. Board 2001 (1) (2007) 102–109.

[17] W.G. Buttlar, P. Rath. Illinois Tollway Project Illinois Tollway I-88 Ground Tire Rubber Test Sections, 2017.

[18] W.G. Buttlar, B.C. Hill, H. Wang, W. Mogawer, Performance space diagram for the evaluation of high- and low-temperature asphalt mixture performance, Road Mater. Pavement Des. 18 (November) (2017) 336–358, https://doi.org/10.1080/14680629.2016.1267446.

[19] W. Buttlar, J. Meister, B. Jahangiri, H. Majidifard. Performance Characteristics of Modern Recycled Asphalt Mixes in Missouri, Including Ground Tire Rubber, Recycled Roofing Shingles, and Rejuvenators. Draft Publication (Under Review), Missouri DOT. in press.

[20] W. Buttlar, P. Rath, E. Dave, H. Majidifard, H. Wang, Relating DC(T) Fracture Energy to Field Cracking Observations and Recommended Specification Thresholds for Performance-Engineered Mix Design, In: Submitted to Transportation Research Circular, Transportation Research Board, 2018.

[21] S.K. Das, Artificial neural networks in geotechnical engineering: modeling and application issues. Metaheuristics in Water, geotechnical and transport engineering, Elsevier, London, 2013.

[22] E.V. Dave, B. Behnia, S. Ahmed, W.G. Buttlar, H. Low, Temperature Fracture Evaluation of Asphalt Mixtures Using Mechanical Testing and Acoustic Emission Techniques, 2013.

[23] E.V. Dave, C. Hoplin, Flexible pavement thermal cracking performance sensitivity to fracture energy variation of asphalt mixtures, Road Mater. Pavement Des. 16 (Suppl. 1) (2015) 423–441.

[24] U. Federal, R. Estadual, E. Superior, R. Estadual, E. Superior. 1, 2 3. 2005, pp. 1–13.

[25] C. Ferreira, Gene expression programming: a new adaptive algorithm for solving problems, Complex Syst. 13 (2001) 87–129.

[26] A.H. Gandomi, A.H. Alavi, M.G. Sahab, New Formulation for Compressive Strength of CFRP Confined Concrete Cylinders Using Linear Genetic Programming Materials and Structures, 43(7), 2010, 963–983.

[27] A. Garg, L. Rachmawatiand, K. Tai, Classification-driven model selection approach of genetic programming in modelling of turning process, Int. J. Adv. Manuf. Technol. 69 (2013) 1137–1151.

[28] A. Garg, X. Peng, M.L. Le, K. Pareek, C. Chin, Design and analysis of capacity models for Lithium-ion battery, Measurement 120 (2018) 114–120.

[29] A. Garg, V. Vijayaraghavan, C.H. Wong, K. Tai, S.S. Mahapatra, Measurement of properties of graphene sheets subjected to drilling operation using computer simulation, Measurement 50 (2014) 50–62.

[30] A. Garg, A. Garg, K. Tai, S. Sreedeep, An integrated SRM-multi-gene genetic programming approach for prediction of factor of safety of 3-D soil nailed slopes, Eng. Appl. Artif. Intell. 30 (2014) 30–40.

[31] A. Garg, K. Shankhwar, D. Jiang, V. Vijayaraghavan, B.N. Panda, S. Panda, An evolutionary framework in modelling of multi-output characteristics of the bone drilling process, Neural Comput. Appl. 10 (2016) 1233–1241.

[32] G.D. Garson, Interpreting neural-network connection weights, AI Expert 6 (1991) 47–51.

[33] R. Ghabchi, D. Singh, M. Zaman, Laboratory evaluation of stiffness, low-temperature cracking, rutting, moisture damage, and fatigue performance of WMA mixes, Road Materi. Pavement Des. 16 (2) (2015) 334–357.
[34] A.T.C. Goh, F.H. Kulhawy, C.G. Chua, Bayesian neural network analysis of undrained side resistance of drilled shafts, ASCE J. Geotech. Geoenviron. Eng. 131 (1) (2005) 84–93.
[35] A. Golbraikh, A. Tropsha, Beware of q2, J. Mol. Graph. Model. 20 (4) (2002) 269–276.
[36] O. Gunaydin, Estimation of soil compaction parameters by using statistical analyses and articial neural networks, Environ. Geol. 10 (2008) 1300{1306.
[37] B. Asphalt Hill, Mixture Evaluation Using Performance Space Diagrams, Digital Image Correlation, and Discrete Element Modeling PhD. Dissertation, University of Illinois at Urbana-Champaign, 2016.
[38] C.M. Hoplin, Cracking Performance Evaluation of Minnesota Asphalt Pavements MSc Thesis, University of Minnesota, 2016.
[39] Y. Huang, L. Gao, Z. Yi, K. Tai, P. Kalita, P. Prapainainar, A. Garg, An application of evolutionary system identification algorithm in modelling of energy production system, Measurement 114 (2018) 122–131.
[40] B. Jahangiri, H. Majidifard, J. Meister, W.G. Buttlar, Performance Evaluation of Asphalt Mixtures with RAP and RAS in Missouri. Accepted to be published in Journal of Transportation Research Record (TRR). In press.
[41] Y.P. Kim, Cohesive zone model to predict fracture in bituminous materials and asphaltic pavements: state-of-the-art review, Int. J. Pavement Eng. 12 (4) (2011) 343–356.
[42] S. Kirkpatrick, C.D. Gelatt, M.P. Vecchi, Optimization by simulated annealing, Science 220 (4598) (1983) 671–680.
[43] J.R. Koza, Genetic Programming, on the Programming of Computers by Means of Natural Selection, MIT Press, Cambridge (MA), 1992.
[44] D.J. Lary, A.H. Alavi, A.L. Walker, A.H. Gandomi, Machine learning in geosciences and remote sensing, Geosci. Front. 7 (2016).
[45] S. Ledesma, M. Torres, D. Hernandez, G. Avina, G. Garcia, Temperature Cycling on Simulated Annealing for Neural Network Learning. In: Proceedings of the MICAI 2007, LNAI 4827, 2007, p. 161–171.
[46] Q. Li, H.J. Lee, T.W. Kim, A simple fatigue performance model of asphalt mixtures based on fracture energy, Constr. Build. Mater. 27 (2012) 605–611.
[47] X.J. Li, M.O. Marasteanu, Using semi circular bending test to evaluate low temperature fracture resistance for asphalt concrete, Exp. Mech. 50 (7) (2010) 867–876, https://doi.org/10.1007/s11340-009-9303-0.
[48] X. Li, A.F. Braham, M.O. Marasteanu, W.G. Buttlar, R.C. Williams, Effect of factors affecting fracture energy of asphalt concrete at low temperature, Road Mater. Pavement Des. 9 (suppl. 1) (2008) 397–416.
[49] T.B. Ludermir. Neural networks for odor recognition in artificial noses. In: Proceedings of the International Joint Conference on Neural Networks, Portland, Oregon, 2003. p. 143–148.
[50] H. Majidifard, N. Tabatabaee, W.G. Buttlar. Investigating Short-term and Long-term Binder Performance of High-RAP Mixtures Containing Waste Cooking Oil. Accepted to be published in Journal of Traffic and Transportation, In press.
[51] M.O. Marasteanu, K.H. Moon, E.Z. Teshale, A.C. Falchetto, M. Turos, W.G. Buttlar, E. Dave, G. Paulino, S. Ahmed, S. Leon, A. Braham, B. Behnia, H. Bahia, H. Tabatabaee, R. Velasquez, A. Arshadi, P. Sebastian, S. Mangiafico, C.R. Williams, A. Buss, J. Bausano, A. Kvasnak, Investigation of low temperature cracking in asphalt pavements, National Pooled Fund Study Phase-II (2012).
[52] M.O. Marasteanu, W.G. Buttlar, H. Bahia, C. Williams, Investigation of Low Temperature Cracking in Asphalt Pavements. Report # MN/RC 2012-23, Minnesota Department of Transportation, 2007.
[53] M.S.M. Medeiros, J.S. Daniel, G.R. Chehab, Framework for low-temperature cracking analysis of asphalt mixtures using a viscoelastic continuum damage model, J. Mater. Civ. Eng. 27 (10) (2014) pp.
[54] Y. Mejias de Pernia, M. Gunaratne, Application of perceptual image coding and the neural network method in predicting the optimum Asphalt binder content of open-graded friction course mixtures, Road Mater. Pavement Des. 18 (1) (2017).
[55] D.J. Mensching, G.M. Rowe, J.S. Daniel, T. Bennert, Exploring low temperature performance in black space, J. Road Mater. Pavement Des. 16 (suppl. 2) (2015).
[56] D.J. Mensching, G.M. Rowe, J.S. Daniel, A mixture-based Black Space parameter for low temperature performance of hot mix asphalt, Road Mater. Pavement Des. 18 (Suppl. 4) (2017) 491–513.
[57] N. Metropolis, A.W. Rosenbluth, M.N. Rosenbluth, A.H. Teller, E. Teller, Equation of state calculations by fast computing mechanics, J. Chem. Phys. 21 (6) (1953) 1087–1092.
[58] M. Miradi, A.A.A. Molenaar, M.F.C. van de Ven, Performance modelling of porous asphalt concrete using artificial intelligence, Road Mater. Pavement Des. ICAM (2009).
[59] T. Mitchell, Does machine learning really work?, AI Mag 18 (3) (1997) 11–20.
[60] W.S. Mogawer, A. Austerman, I.L. Al-Qadi, W. Buttlar, H. Ozer, B. Hill, Using binder and mixture space diagrams to evaluate the effect of re-refined engine oil bottoms on binders and mixtures after ageing, Road Mater. Pavement Des. 18 (April) (2017) 154–182.
[61] S.M. Mousavi, E.S. Mostafavi, P. Jiao, Next generation prediction model for daily solar radiation on horizontal surface using a hybrid neural network and simulated annealing method, Energy Convers. Manage. (2014).
[62] S.M. Mousavi, A.H. Gandomi, A.H. Alavi, M. Vesalimahmood, Modeling of compressive strength of HPC mixes using a combined algorithm of genetic programming and orthogonal least squares, Struct. Eng. Mech. 36 (2) (2010) 225–241.
[63] P.K. Muduli, S.K. Das, S. Bhattacharya, CPT-based probabilistic evaluation of seis- mic soil liquefaction potential using, multi-gene genetic programming, Georisk 8 (1) (2014) 14–28.
[64] O. Onal, A.U. Ozturk, Artificial neural network application on microstructure–compressive strength relationship of cement mortar, Adv. Eng. Softw. 41 (2010) 165–169.
[65] T.S. Ozsahin, S. Oruc, Neural network model for resilient modulus of emulsified asphalt mixtures, Constr. Build. Mater. 22 (2008) 1436–1445.
[66] H.I. Park, G.C. Kweon, S.R. Lee, Prediction of resilient modulus of granular subgrade soils and subbase materials using artificial neural network, Road Mater. Pavement Des. 10 (3) (2009).
[67] M. Parvini, Artificial neural network modeling of pavement performance using expert judgement, Road Mater. Pavement Des. 3 (4) (2002).
[68] V.W. Porto, D.B. Fogel, L.J. Fogel, Alternative neural network training models, IEEE Expert (1995) 16–22.
[69] M.Y. Rafiq, G. Bugmann, D.J. Easterbrook, Neural network design for engineering applications, Comput. Struct. 79 (2001) 1541–1552.
[70] R. Rahbar-rastegar, E.V. Dave, J.S. Daniel, Fatigue and thermal cracking analysis of asphalt mixtures using continuum-damage and cohesive-zone models, 144 (4), 2018, pp. 1–11.
[71] P.M. Ramos, F.M. Janeiro, Gene expression programming for automatic circuit model identification in impedance spectroscopy: performance evaluation, Measurement 46 (2013) 4379–4387.
[72] L.M.R. Rere, M.I. Fanany, A.M. Arymurthy, Simulated annealing algorithm for deep learning, Procedia Comput. Sci. 72 (2015) 37–144.
[73] P.P. Roy, K. Roy, On some aspects of variable selection for partial least squares regression models, QSAR Comb. Sci. 27 (3) (2008) 302–313.
[74] D.E. Rumelhart, J.L. McClelland, Parallel distributed processing, Vol. 1: Foundations, The MIT Press, Cambrdige, MA, 1986.
[75] E. Sadrossadat, A. Heidaripanah, B. Ghorbani, Towards application of linear genetic programming for indirect estimation of the resilient modulus of pavements subgrade soils, Road Mater Pavement (19. 2018.).
[76] M. Saltan, H. Sezgin, Hybrid neural network and finite element modeling of subbase layer material properties in flexible pavements, Mater Des. 28 (2007) 1725–1730.
[77] M. Saltan, S. Terzi, Modeling deflection basin using artificial neural networks with cross-validation technique in back calculating flexible pavement layer moduli, Adv. Eng. Soft 39 (2008) 588–592.
[78] P. Samui, Application of statistical learning algorithms to ultimate bearing capacity of shallow foundation on cohesionless soil, Int. J. Numer. Anal. Meth. Geomech. 36 (1) (2012) 100–110.
[79] P. Samui, Support vector machine applied to settlement of shallow foundations on cohesionless soils, Comput. Geotech. 35 (3) (2008) 419–427.
[80] A. Sarfaraz, Fracture Characterization of Thin Bonded Asphalt Concrete Overlay Systems PhD. Dissertation, University of Illinois at Urbana-Champaign, 2011.
[81] M. Sarıdemir, Prediction of compressive strength of concretes containing metakaolin and silica fume by artificial neural networks, Adv. Eng. Softw. 40 (2009) 350–355.
[82] R.S. Sexton, B. Alidaee, R.E. Dorsey, J.D. Johnson, Global optimization for artificial neural networks: a tabu search application, Eur.o J. Operation Res. 06 (2–3) (1998) 570–584.
[83] M.A. Shahin, H.R. Maier, M.B. Jaksa, Artificial neural network applications in geotechnical engineering, Austr. Geomech. 36 (2001) 49–62.
[84] G.N. Smith, Probability and statistics in civil engineering, Collins, London, 1986.
[85] S.H. Song, G.H. Paulino, W.G. Buttlar, A bilinear cohesive zone model tailored for fracture of asphalt concrete considering viscoelastic bulk material, J. Eng. Fract. Mech. 73 (2006) 2829–2848.
[86] K. Swingler, Applying Neural Networks a Practical Guide, Academic Press, USA, New York, 1996.
[87] J.A. Torkestani, An adaptive learning automata-based ranking function discovery algorithm, J. Intell. Inform. Syst. 39 (2012) 441–459.
[88] M. Wagoner, W. Buttlar, G. Paulino, P. Blankenship, Investigation of the fracture resistance of hot-mix asphalt concrete using a disk-shaped compact tension test, Transp. Res. Rec. 1929 (1) (2005) 183–192, https://doi.org/10.3141/1929-22.
[89] X. Yang, Z. You, M.R.M. Hasan, A. Diab, H. Shao, S. Chen, D. Ge, Environmental and mechanical performance of crumb rubber modified warm mix asphalt using evotherm, J. Cleaner Prod. 159 (2017) 346–358, https://doi.org/10.1016/j.jclepro.2017.04.168.
[90] E.T. Zegeye, K.H. Moon, M. Turos, T.R. Clyne, M.O. Marasteanu, Low Temperature Fracture Properties of Polyphosphoric Acid Modified Asphalt Mixtures 24, August, 2012, pp. 1089–1096.
[91] H. Zhang, T. Yu, Prediction of subgrade elastic moduli in different seasons based on BP neural network technology, Road Mater. Pavement Des. 19 (2) (2018).